Article

Improved Antibacterial Activity of Peptide Nisin with Pyrrole-Based Ionic Liquids Having Bis(trifluoromethylsulfonyl)imide as a Counterion: A Synergistic Approach to Combat Bacterial Infections

Juhi Saraswat, Ahmad Firoz, Majid Rasool Kamli, and Rajan Patel*

Cite This: ACS Omega 2024, 9, 2758−2769

Read Online

ACCESS | Metrics & More | Article Recommendations | SI Supporting Information

ABSTRACT: Bacterial resistance against antimicrobial drugs is a forthcoming threat to the prevention and treatment of developing bacterial infections. Hence, the development of new antimicrobial therapy or therapeutic drugs is desperately needed. A combination of antibiotics exhibits synergistic antibacterial effects. As the combination approach of antibiotics has always shown better results against pathogens compared to monotherapy with an antibiotic, we focused on creating a new combination that may reduce the chances of strains attaining resistance, consequently lowering the toxicity factor associated with the consumption of high amounts of antibiotics. Nisin, a food preservative and potential antibiotic, shows antibacterial activity against Gram-positive strains. Since the past decade, ionic liquids (ILs) have proven to be an important class of potential antibacterial agents. In our study, we studied the effect of pyrrolidinium-based ILs and arrived at a noncovalent conjugate formed by combining nisin with ILs. The conjugates were tested against a couple of clinically relevant microorganisms, namely, *Escherichia coli* and *Staphylococcus aureus*. We reached a novel discovery that the combination of sodium/iodide symporter (NIS) and IL exhibited inhibitory effects against Gram-negative bacteria, which was not observed with NIS alone. The results showed remarkable improvement in the minimum inhibitory concentration (MIC) value of NIS in the presence of ILs targeted against both microorganisms. Further, flow cytometry and confocal microscopy results revealed the membrane disruption efficiency of the best combination obtained, leading to cell death. Additionally, the complexation of nisin and ILs was studied using various techniques, such as surface tension, dynamic light scattering, absorption spectroscopy, and molecular docking.
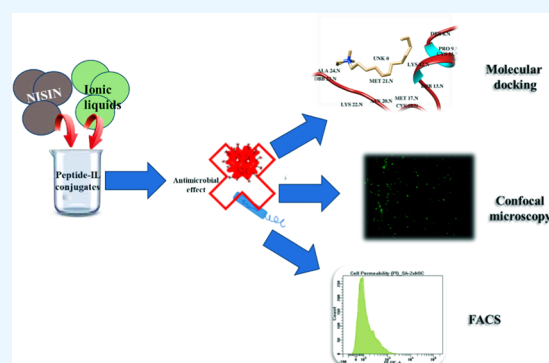
1. INTRODUCTION

Bacterial resistance is responsible for thousands of deaths and longer hospital stays annually due to the failure of antibiotic treatment.[1] Resistant *Escherichia coli* and *Staphylococcus aureus* are human pathogens that can cause a wide range of illnesses related to skin infections and some severe diseases such as pneumonia, sepsis, bacterial infections, viz. cholecystitis, cholangitis, bacteremia, urinary tract infection (UTI), etc. Presently, the crisis of novel antibiotics has become a major concern and challenge for researchers. However, the limited availability of novel antibiotics leads to the evolution of pathogen resistance.[2] Based on a survey of multidrug resistance (MDR) of pathogens, developing new strategies or combination therapies for the effective treatment of resistant bacteria has become a major concern of researchers. The current trend shows that antimicrobial peptides (AMPs) are extensively used as a new class of antibacterial drugs due to their characteristics, such as enhanced antibiotic potency and lower propensity for resistance.[3] Therefore, AMPs may be considered as promising alternatives to current antibiotics or as good candidates to enhance antibiotic potency. Additionally, the use of ionic

liquids can enhance the antibacterial activity of antibiotics.[4] Although ionic liquids (ILs) are potential antibiotics for the treatment of various infections, conventional antibiotics today are prime sources for treatment and cannot be replaced fully. Therefore, combining them with antibiotics (AMPs) can increase the life span and also increase the antibacterial activity of antibiotics.[5]

Nisin is a cationic polypeptide containing 34 amino acids, which originates from *Lactococcus lactis* and is minimally toxic, odorless, colorless, and tasteless.[6] Naturally occurring nisin Z has asparagine at the 27 position, which differentiates it from other variants of nisin, such as nisin A, which consists of histidine at the 27 position.[7] It has already been reported that both have similar antimicrobial activities. As reported earlier,
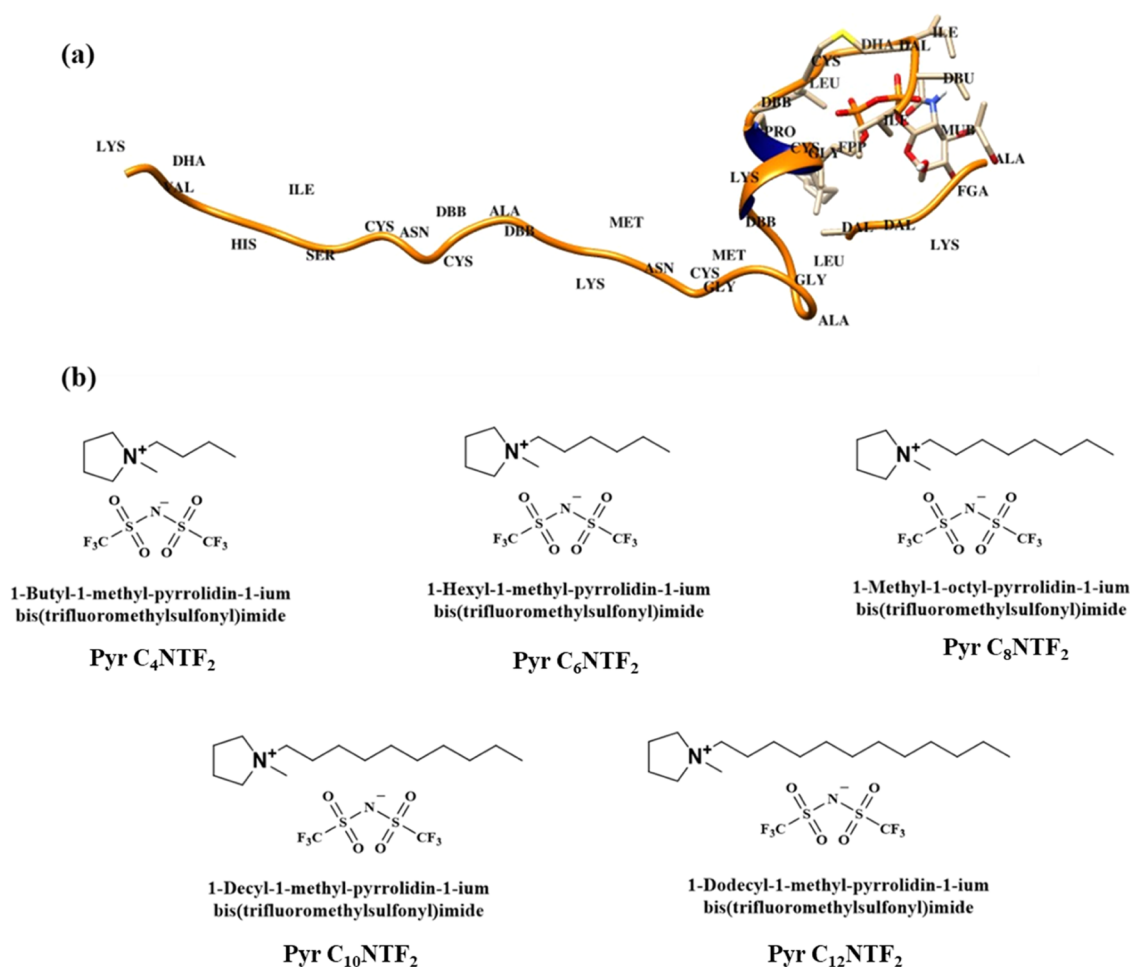
Figure 1. (a) Structure of nisin Z (PDB ID: 1WCO). (b) Chemical structure of pyrrole-based ILs having bis(trifluoromethylsulfonyl)imide as a counterion.

nisin is an effective AMP against the growth of drug-resistant strains such as methicillin-resistant *S. aureus* and *Clostridium difficile*.[8] Various groups of researchers have worked on combinations of nisin with antibiotics.[1,9] In order to improve the therapeutic potential of nisin, combining nisin with ionic liquids can be considered an efficient therapeutic strategy against resistant pathogens.

Ionic liquids (ILs), for a long time, have gained considerable attention of researchers from various fields due to their exceptional characteristic features, such as negligible vapor pressure, tunability, low volatility, nonflammability, antibacterial properties, etc. (Hodyna et al.,). ILs consist of organic cations and anions. In recent years, the toxicity of ILs to organisms and nature has been well reported.[10] Therefore, we synthesized a series of pyrrolidinium-based ILs that possess lesser toxicity compared to imidazolium- and pyridinium-based ILs.[11] A combination of two antibiotics, pyrrole-based ILs and nisin Z, can suppress antibacterial resistance compared to treatment with individual antibiotics.

Therefore, the present study aims to evaluate the antibacterial activities of nisin and the combination of pyrrolidinium-based ILs with nisin against two microorganisms, *E. coli* and *S. aureus* strains, grown under anaerobic conditions, thus exploring the feasibility of combinations of ILs and nisin against drug resistance. The combined approach of two antibiotics has been studied extensively, but the combination therapy of nisin and ILs has not yet been

explored. Also, a binding study was performed to investigate the complex formation between sodium/iodide symporter (NIS) and ILs using various techniques such as molecular docking, dynamic light scattering, absorption spectroscopy, and surface tension. Additionally, the effect of ILs on the secondary structure of NIS was studied in order to investigate the change in the secondary structure of NIS with the addition of ILs. In the end, a hemocompatibility assay was performed to evaluate the compatibility of the designed conjugates of NIS–IL with human serum albumin (HSA).

2. MATERIALS AND METHODS

2.1. Materials. Nisin Z (purity ≥98%) (Figure 1a) was purchased from Sigma-Aldrich. Luria−Bertani broth (LBB), *E. coli* (MTCC 40), and *S. aureus* (MTCC 87) cultures were obtained from the microbial type culture collection and gene bank (MTCC), CSIR-Institute of microbial technology, Chandigarh, India. The ILs used in present study were 1-butyl-1-methylpyrrolidin-1-ium bis(trifluoromethylsulfonyl)-imide [Pyr C_4]NTF$_2$, 1-hexyl-1-methylpyrrolidin-1-ium bis-(trifluoromethylsulfonyl)imide [Pyr C_6]NTF$_2$, 1-methyl-1-octylpyrrolidin-1-ium bis(trifluoromethylsulfonyl)imide [Pyr C_8]NTF$_2$, 1-decyl-1-methylpyrrolidin-1-ium bis-(trifluoromethylsulfonyl)imide [Pyr C_{10}]NTF$_2$, and 1-dodec-yl-1-methylpyrrolidin-1-ium bis(trifluoromethylsulfonyl)imide [Pyr C_{12}] NTF$_2$ (Figure 1b), which were synthesized in our

laboratory.[12] Ethanol, glycerol, and autoclaved water were used to study the antibacterial activity, while Milli-Q water was used for the spectroscopic and tensiometry experiments.

2.1.1. Preparation of the Bacterial Inoculum. The two strains were routinely revived in Luria−Bertani broth (LBB) and cultured under anaerobic conditions in an orbital shaker at 37 °C for 18 h up to the logarithmic phase. The optical density of both strains was measured to determine the growth using Analytikjena 210 (Germany) at 600 nm (OD_{600}). The obtained OD_{600} was 0.54. The working concentration of the inoculum ($OD_{600} = 0.54$) was adjusted to $10^6 - 10^5$ CFU/mL.

2.1.2. Preparation of Resazurin (Dye). The resazurin dye solution was prepared by thoroughly mixing 0.015 g of resazurin (dye) in 100 mL of autoclaved water. The prepared solution was vortexed, filtered with a 0.22 mm filter, and stored at 4 °C for a maximum of 2 weeks after its preparation.

2.2. Methods. *2.2.1. Determining the Minimum Inhibitory Concentration (MIC).* The MIC of NIS was evaluated using the microplate dilution method in LBB by following the recommendations of the Clinical and Laboratory Standards Institute.[13] In brief, the stock solution of nisin Z was 2-fold serially diluted (100 μL) along the *x*-axis in a 96-well plate. After the addition of the antibiotic, 10 μL of bacterial suspension, whose working concentration was adjusted to $10^5 - 10^6$ CFU/mL, was added to each well except the sterile control (SC). Luria−Bertani broth (LBB) with and without the bacterial inoculum served as the growth control (GC) and sterile control, respectively. The plates were incubated at 37 °C for 16−18 h. After incubation, 10 μL of resazurin (0.015%) was added to each well. The plate was incubated for another 3−4 h for color change, if any. In column 12 (a−d), the growth control shows a change in the natural color of resazurin (blue/purple) to that of the reduced form (red/colorless). The absence of color change in column 12 (e−h) suggested that no contamination occurred during the preparation of the plate. Further results were analyzed on the basis of color change, as reported earlier.[14] All tests were performed in triplicate for each experiment on MIC determination. The MIC value of IL used in the current study was previously determined and is reported in our previous publication.[12]

2.2.2. Effect of IL on NIS. To investigate the effect of ILs on the activity of nisin Z, a checkerboard assay was performed by following a procedure reported in the literature.[1,15] In brief, the stock solution of NIS was 2-fold serially diluted to maintain the concentration in the range of 180−0.008 μM along the *y*-axis in the 96-well plate. The column contained the same concentration of nisin Z, and thereafter, various concentrations of ILs ([Pyr C_4]NTF$_2$ (10, 20, 50, 100, and 200 μM), [Pyr C_6]NTF$_2$ (2, 5, 10, 50, and 100 μM), [Pyr C_8]NTF$_2$ (1, 5, 10, 20, and 50 μM), [Pyr C_{10}]NTF$_2$ (5, 10, 50, 100, and 150 μM), and [Pyr C_{12}]NTF$_2$ (0.5, 1, 5, 10, and 20 μM)) were added column-wise. Thereafter, 10 μL of the bacterial inoculum, whose working concentration was adjusted to $10^5 - 10^6$ CFU/mL, was added to each well in a 96-well plate. LBB with and without the bacterial inoculum served as the growth control (GC) and sterile control (SC), respectively. The plate was incubated at 37 °C for 16−18 h. Separate plates were prepared for each experiment. The optical density (OD_{600}) was recorded and plotted against the concentration of antibiotic using a microplate reader. Thereafter, 10 μL of resazurin (0.015%) was added to each well. The plates were incubated for another 3−4 h for color change, if any. Column 12 (a−d), the negative control (growth control), showed a change in the natural color

of resazurin (blue/purple) to that of the reduced form (red/colorless). Column 12 (e−h) shows no color change, which confirms that no contamination occurred while preparing the plate. Further results were analyzed on the basis of color change, as reported earlier.[14] All tests were performed in triplicate for each experiment on MIC determination. Further, the membrane destruction potential of the NIS peptide and NIS−[Pyr C_{12}]NTF$_2$ (best combination obtained) against bacteria was determined using the fluorescence-activated cell sorting (FACS) technique, as discussed in the upcoming section. Additionally, bacterial cells were visualized after treatment with the NIS peptide and NIS−[Pyr C_{12}]NTF$_2$ (best combination obtained). Staining of dead cells using propidium iodide (PI) was performed, and confocal laser scanning microscopy (CLSM) helped visualize the effectiveness of treatment against bacterial strains.

2.2.3. Fluorescence-Activated Cell Sorting (FACS). A membrane permeability assay was carried out using the fluorescence-activated cell sorting technique.[16] The cell membrane disruption of microorganisms, *E. coli* and *S. aureus*, after the treatment with NIS and its best combination was analyzed using the propidium iodide (PI) assay, as described previously.[16] The treated *E. coli* MTCC 40 and *S. aureus* MTCC 87 strains were incubated for their growth up to the logarithmic phase at 37 °C for 18 h. The treated samples were centrifuged at 13,000 rpm for 15 min. The cells in the form of pellets were washed thrice with phosphate buffer (10 mM, 7.4 pH). The working cell concentration was adjusted to 10^5 CFU/mL. 10 μL of 20 μM propidium iodide (dye) was added to each sample, except the unstrained sample (growth control), followed by the incubation of the samples in the dark for 30 min. The data were recorded on a FACS instrument (BD FACSAria-III). The laser excitation wavelength was kept at 488 nm. The recorded data were analyzed using BD FACSDiva 8.0.3 software.

2.2.4. Confocal Laser Scanning Microscopy (CLSM). CLSM technique was used to visualize the bacterial cell membrane after treatment with NIS and its best combination with IL. Staining of live/dead bacterial cells using propidium iodide was carried out as reported in the literature.[17] Cells of *E. coli* and *S. aureus* were treated with NIS and its conjugates at 37 °C for 18 h. After treatment, the samples were centrifuged for 10 min at 13,000 rpm Thereafter, the obtained pellets of samples were washed thrice using phosphate buffer (10 mM. 7.4 pH). The cell concentration was kept at 10^6 CFU/mL for the measurement. 10 μL of PI (20 μM) was added to each sample, including the control. Samples were incubated in the dark for 1 h. After incubation, the samples were vortexed, and one drop of the sample was cast on a glass slide and covered with a coverslip. The coverslip was sealed using a bond primer.[17] Slides prepared were analyzed using a Leica Microsystems TCS SP8 Leica DMi8 microscope. The software used to capture and process images was Leica Application Suite X. The scan speed was 200 Hz, and the magnification was set to 63. A 488 nm laser was used, and the emission was recorded between 580 and 670 nm. The transmission channel was PMT.

2.2.5. Molecular Docking. The molecular docking technique was performed using AutoDock tool 1.5.6 by employing the Lamarckian Genetic Algorithm.[18] The pdb structure of NIS was obtained from an online protein data bank (pdb) (http://www.rcsb.org/, PDB ID: 1WCO). The structure of NIS was obtained by removing the lipid from the .pdb file

Table 1. Best Combinations of Synthesized Pyrrolidinium-Based ILs with NIS

s.no.	combinations	against *E. coli*	against *S. aureus*
1.	NIS	22.5 μM	1.40 μM
2.	NIS + [Pyr C$_4$] NTF$_2$	11.86 μM + 100 μM	1.37 μM + 100 μM
3.	NIS + [Pyr C$_6$] NTF$_2$	5.44 μM + 100 μM	1.21 μM + 50 μM
4.	NIS + [Pyr C$_8$] NTF$_2$	2.72 μM + 50 μM	0.29 μM + 20 μM
5.	NIS + [Pyr C$_{10}$] NTF$_2$	2.42 μM + 10 μM	0.28 μM + 5 μM
6.	NIS + [Pyr C$_{12}$]NTF$_2$	2.23 μM + 5 μM	0.21 μM + 2 μM

using PyMol software. The NIS structure was assigned the Kollman charges and AD4-type atoms along with polar hydrogen atoms. The structure of the IL was drawn with ChemDraw Ultra 8.0 and was converted to the pdb format using Chem3D Ultra 8.0 software. The grid map was generated. A total of 100 runs were carried out to dock the IL with NIS. The dimensions of the grid were 50 × 46 × 54. The grid spacing was kept at 0.375 Å. After the completion of runs, the most favorable conformation was selected based on the binding energy and the favorable geometry. Further, for visualization, Discovery Studio (BIOVIA-2016) and Chimera 1.12 software were used.[19]

Based on the best-fit score (minimum binding energy) (given in Table S1) of all five ILs, the best binding was obtained between NIS and [Pyr C$_{12}$] NTF$_2$ after a molecular docking analysis. Further, a detailed study of the interaction between NIS and [Pyr C$_{12}$] NTF$_2$ was conducted using various techniques such as surface tension, dynamic light scattering, etc., which are discussed in the upcoming sections.

2.2.6. Surface Tension. The surface tension of [Pyr C$_{12}$]NTF$_2$ in the absence and presence of NIS (50 μM) was recorded on a DeltaPi-4 Langmuir microtensiometer, Kibron, Helsinki, Finland, at 298 K. [Pyr C$_{12}$]NTF$_2$ was added to 50 μM NIS by the titration method. The temperature of the sample stage was maintained using a thermostat, GD120, with a temperature variability of ±0.15 K. The tensiometer was equipped with microbalances containing a special alloy wire of radius 0.25 nm, which acts as a probe. A multiwell plate made up of Teflon, containing wells of radius 0.25 nm, was used to measure the surface tension. The capacity of each well in the plate was 1 mL.[20]

2.2.7. Turbidity Measurement. The absorbance at 600 nm of NIS (50 μM) in the absence and presence of [Pyr C$_{12}$]NTF$_2$ was measured using a UV–vis spectrophotometer (Analytikjena Specord-250 spectrophotometer, Germany) at 37 °C. The temperature of the sample cell was maintained using a thermostat, Analytikajena. The samples were prepared in phosphate buffer at a pH of 7.2. The concentration of [Pyr C$_{12}$] NTF$_2$ was varied from 0.05 to 0.6 mM.

2.2.8. Dynamic Light Scattering (DLS) Measurement. The average size of the aggregate of the IL [Pyr C$_{12}$]NTF$_2$ in the absence and presence of NIS was measured by dynamic light scattering. DLS was performed at a scattering angle of 173° using a Malvern Zeta sizer Nano-ZS instrument. The instrument was fitted with a He–Ne laser (λ = 632.8 nm). The working concentration of NIS was 50 μM, and the concentration was varied from 0.05 to 0.6 mM. Each sample was filtered through a 0.22 μM pore size microfilter. A total of three accumulations were set while performing the experiment.

2.2.9. Circular Dichroism. The far-UV CD spectra of NIS (50 μM) in the absence and presence of [Pyr C$_{12}$]NTF$_2$ were recorded on a Cary Eclipse spectrophotometer (Varian), which was fitted with a 150 W xenon lamp. The temperature of the

sample holder was controlled using a Peltier control temperature device and was set at 25 °C. The CD spectra of the samples were recorded using a 0.1 cm quartz cuvette. The sample was prepared in phosphate buffer at a pH of 7.2. The concentration of [Pyr C$_{12}$]NTF$_2$ was varied from 0.005 to 0.4 μM.

2.2.10. Hemocompatibility. To evaluate the effect of the studied combination on human serum albumin, a hemocompatibility assay was performed using various techniques, viz. UV–vis spectroscopy, fluorescence spectroscopy, and far-UV CD spectroscopy, as reported in the literature.[21] The samples prepared included HSA(5 μM), HSA(5 μM)−NIS(50 μM), HSA(5 μM)−NIS(50 μM)−[Pyr C$_4$]NTF$_2$(0.005 μM), HSA(5 μM)−NIS(50 μM)−[Pyr C$_6$]NTF$_2$ (0.05 μM), HSA(5 μM)−NIS(50 μM)−[Pyr C$_8$]NTF$_2$ (0.1 μM), HSA(5 μM)−NIS(50 μM)−[Pyr C$_{10}$]NTF$_2$(0.2 μM), and HSA(5 μM)−NIS(50 μM)−[Pyr C$_{12}$]NTF$_2$ (0.4 μM). All samples were incubated at room temperature for 30 min. Thereafter, UV–vis, fluorescence, and far-UV CD spectra of the aforesaid samples were recorded on the same instruments. For recording the absorption spectra, the range was set to 200−400 nm, keeping the slit width constant at 1 nm throughout the experiment. Fluorescence spectra of the same set of samples were recorded between 290 and 500 nm, keeping the excitation wavelength at 280 nm and slit width constant at 5 nm throughout the experiment. Further, the far-UV CD spectra of the same set of samples were recorded at room temperature within the range of 190−250 nm.

2.2.11. Effect of IL on the Conformation of NIS. The change in the secondary structure of NIS in the presence of ILs was investigated using far-UV CD spectroscopy. The CD signal was recorded within the range of 200−250 nm using a quartz cuvette of 1 cm path length on the same CD spectrophotometer as earlier used. The ellipticities at 222 and 207 nm were considered to calculate the value of *R*, where *R* is the quantitative value for representing any change in the secondary structure of NIS induced due to ILs. The value of *R* was calculated using the equation

$$R = \frac{[\theta]_{222}}{[\theta]_{207}}$$

(1)

where $[\theta]_{207}$ and $[\theta]_{222}$ are the absolute molar ellipticity at wavelengths of 207 and 222 nm, respectively, observed experimentally.

3. RESULTS

3.1. Minimum Inhibitory Concentration Determination. Two strains, *E. coli* and *S. aureus*, were selected, and the activity of NIS was determined by analyzing the reduction in the bacterial burden in terms of the MIC value of NIS. The MIC values of nisin Z against *E. coli* and *S. aureus* were found to be 22.5 and 1.40 μM, respectively. The MIC values of ILs against *E. coli* and *S. aureus* used in the study were earlier
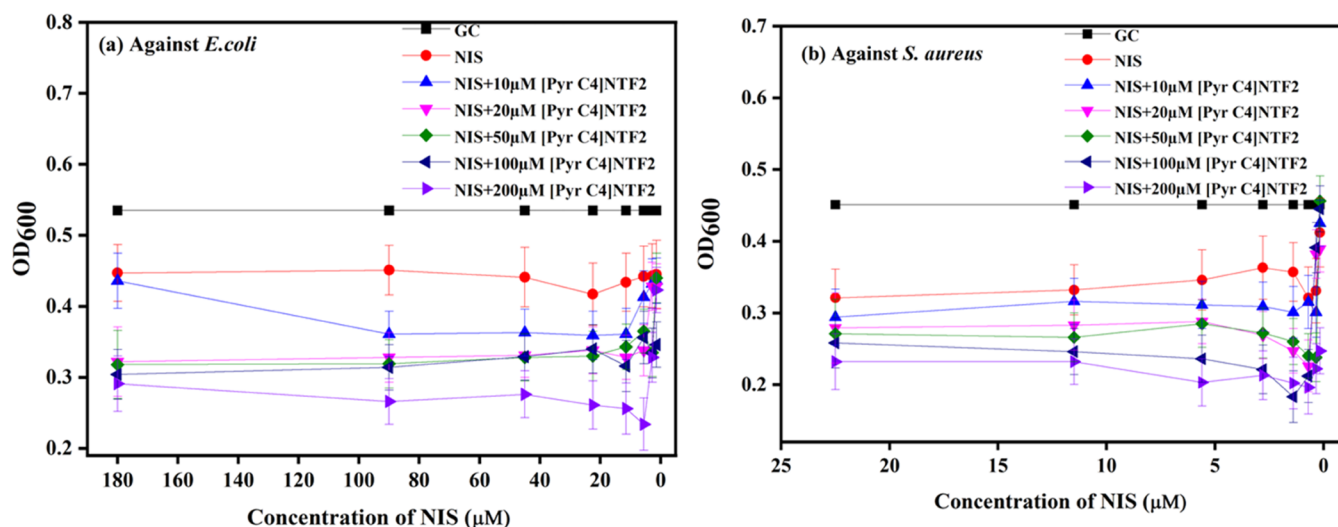
Figure 2. Effect of $[\text{Pyr C}_4]\text{NTF}_2$ concentration on the antibacterial activity of NIS against (a) *E. coli* and (b) *S. aureus*.
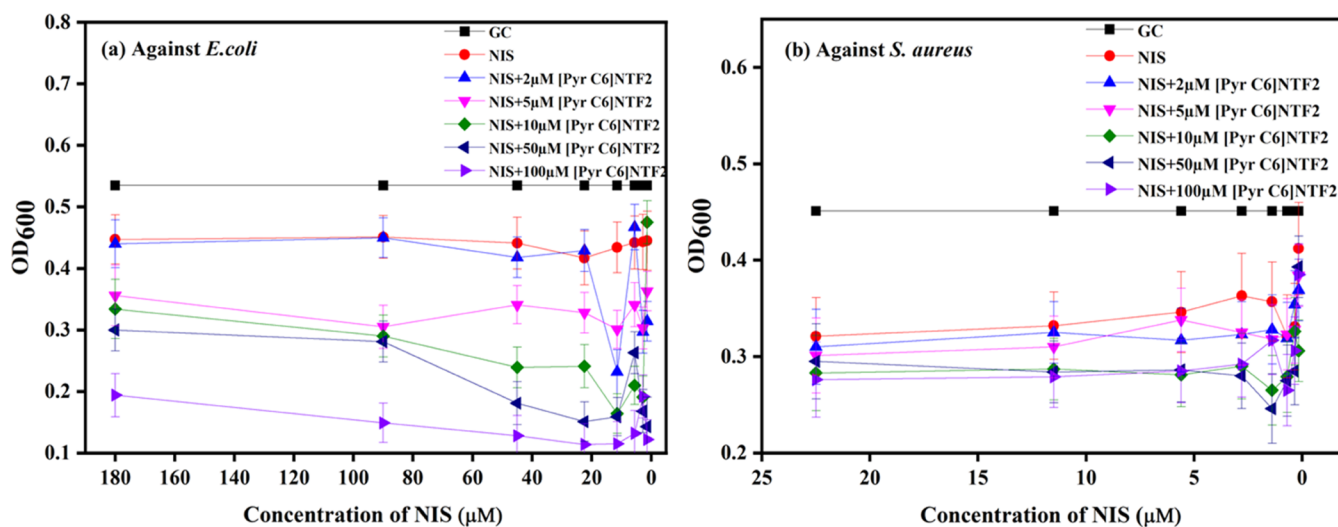
Figure 3. Effect of $[\text{Pyr C}_6]\text{NTF}_2$ concentration on the antibacterial activity of NIS against (a) *E. coli* and (b) *S. aureus*.
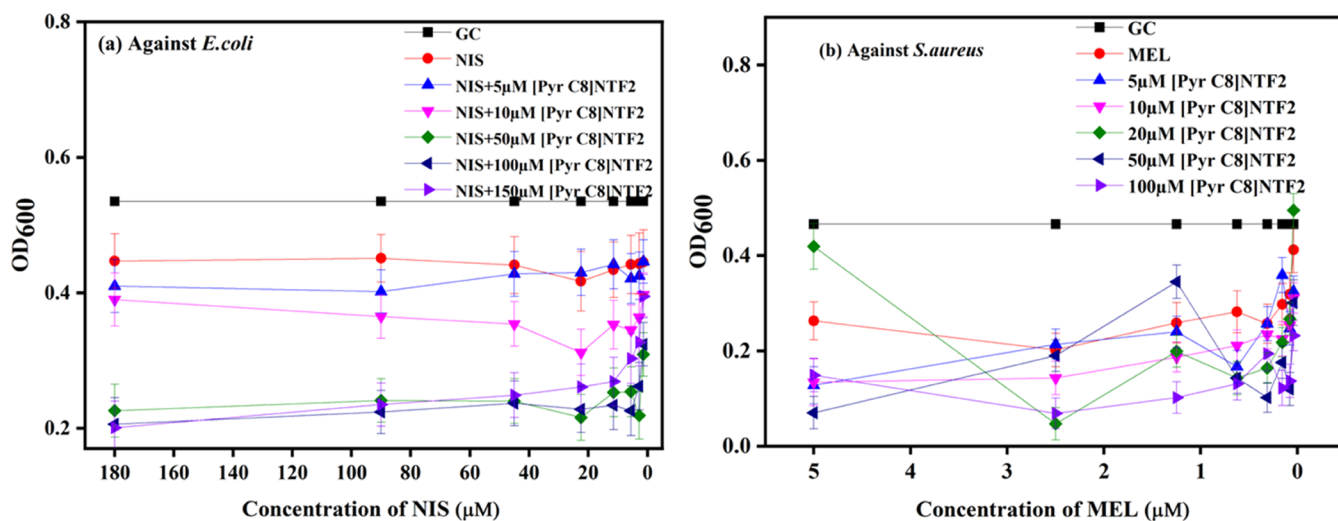
Figure 4. Effect of $[\text{Pyr C}_8]\text{NTF}_2$ concentration on the antibacterial activity of NIS against (a) *E. coli* and (b) *S. aureus*.

determined and have been reported in the literature.[12] The MIC values are summarized in Table 1.

3.2. Biological Activity of NIS in the Presence of ILs.
As earlier reported, the consumption of a higher dosage of
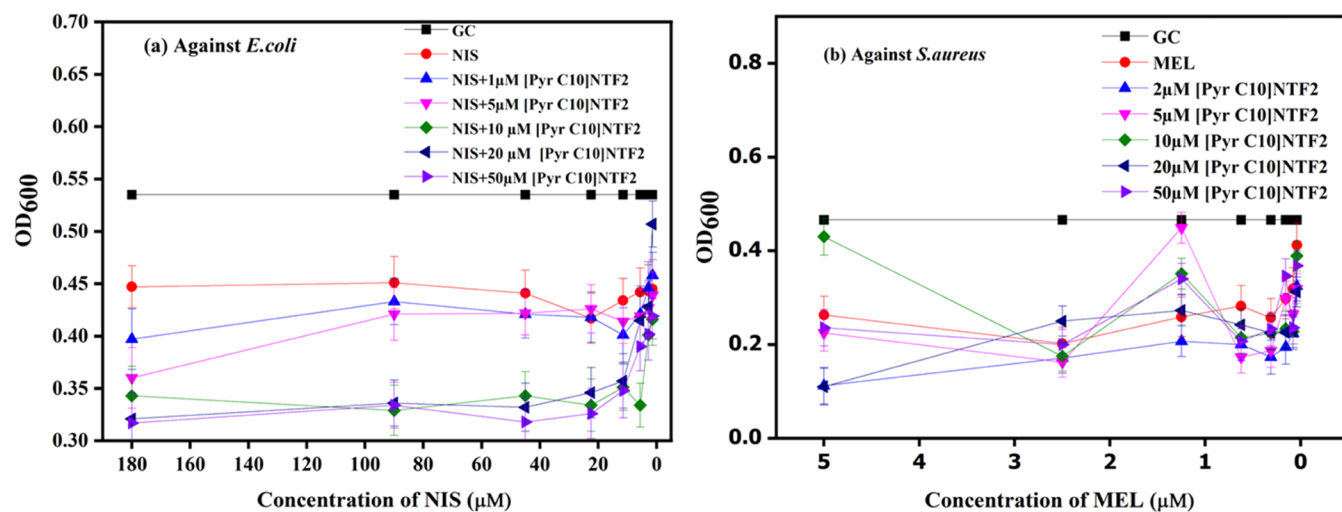
Figure 5. Effect of $[Pyr\ C_{10}]NTF_2$ concentration on the antibacterial activity of NIS against (a) *E. coli* and (b) *S. aureus*.
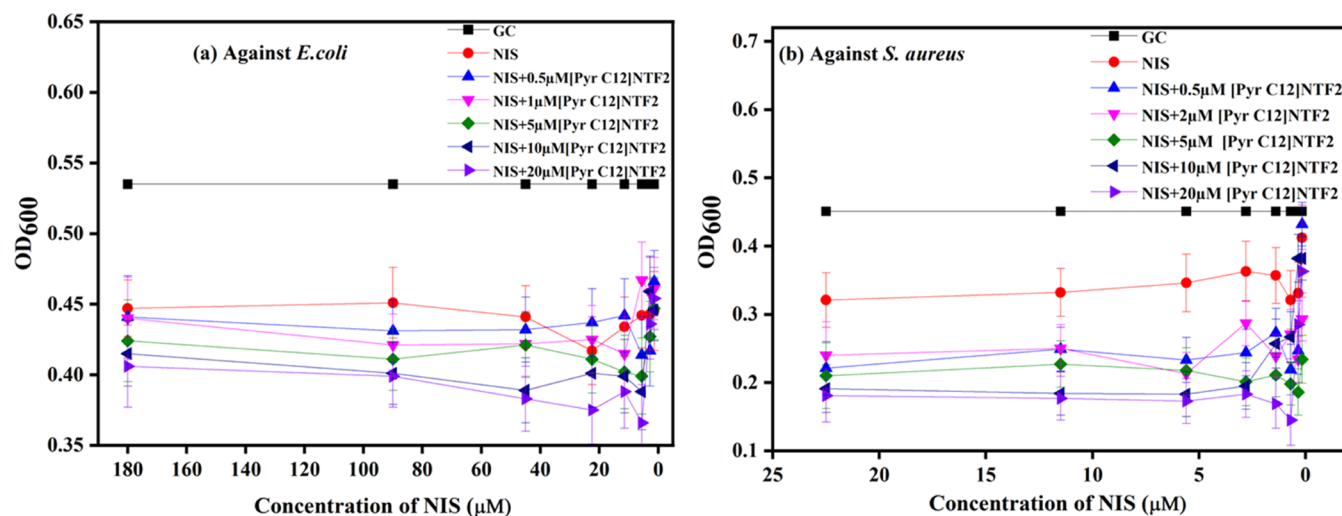
Figure 6. Effect of $[Pyr\ C_{12}]NTF_2$ concentration on the antibacterial activity of NIS against (a) *E. coli* and (b) *S. aureus*.

antibiotics causes various side effects and also results in bacterial resistance.[22] Therefore, various combinations of nisin Z and pyrrolidinium-based ILs were tested to improve the antibacterial properties of nisin Z against *E. coli* and *S aureus*. The reduction in bacterial burden was analyzed in the presence of NIS and its conjugates with ILs. Figures 2−6(a,b) show the growth curves of bacteria *E. coli* and *S. aureus* in the presence of NIS and its conjugates with ILs. In the assay, the MIC of NIS was reduced from 22.5 to 11.86 μM in the presence of 100 μM $[Pyr\ C_4]\ NTF_2$ against *E. coli*, as shown in Figure 2a, whereas it was 1.40−1.37 μM in the presence of 100 μM $[Pyr\ C_4]\ NTF_2$ against *S. aureus*, as shown in Figure 2b.

The MIC of NIS was reduced from 22.5 to 5.40 μM in the presence of 100 μM $[Pyr\ C_6]\ NTF_2$ against *E. coli*, as shown in Figure 3a.

However, it was 1.40−1.21 μM in the presence of 50 μM $[Pyr\ C_6]\ NTF_2$ against *S. aureus*. The MIC of NIS was reduced from 22.5 to 2.72 μM in the presence of 50 μM $[Pyr\ C_8]NTF_2$ against *E. coli* (Figure 4a), whereas it was reduced from 1.40 to 0.29 μM in the presence of 20 μM $[Pyr\ C_8]\ NTF_2$ against *S. aureus* (Figure 4b).

The MIC of NIS was reduced from 22.5 to 2.42 μM in the presence of 10 μM $[Pyr\ C_{10}]\ NTF_2$ against *E. coli* (Figure 5a),

whereas it was reduced from 1.40 to 0.28 μM in the presence of 5 μM $[Pyr\ C_{10}]\ NTF_2$ against *S. aureus* (Figure 5b).

The MIC of NIS was reduced from 22.5 to 0.23 μM in the presence of 5 μM $[Pyr\ C_{12}]\ NTF_2$ against *E. coli* (Figure 6a), whereas it was reduced from 1.40 to 0.21 μM in the presence of 2 μM $[Pyr\ C_{12}]\ NTF_2$ against *S. aureus* (Figure 6b).

As the results suggest, there was a remarkable improvement in the antibacterial activity of NIS in the presence of ILs, but the maximum improvement in the MIC value was observed in the presence of $[Pyr\ C_{12}]\ NTF_2$. The decrease in the MIC value of NIS in the presence of ILs showed a trend. With an increasing number of carbon chains in ILs, the efficacy of NIS improved much more compared to ILs with fewer carbon chains, which was similar to our previously reported data.[12,23,24] This may be due to increasing hydrophobicity, which allows hydrophobic interactions with the cell membrane. NIS at the physiological pH of 7.4 is cationic, where the positive charge in the bulk resides at the C-terminal of the peptide, due to which it becomes the center of attraction for the negatively charged entities, viz., the cell membrane. However, the N-terminus is hydrophobic, which tends to form hydrophobic interactions with the surfactant/ILs, as reported in the literature.[25,26]
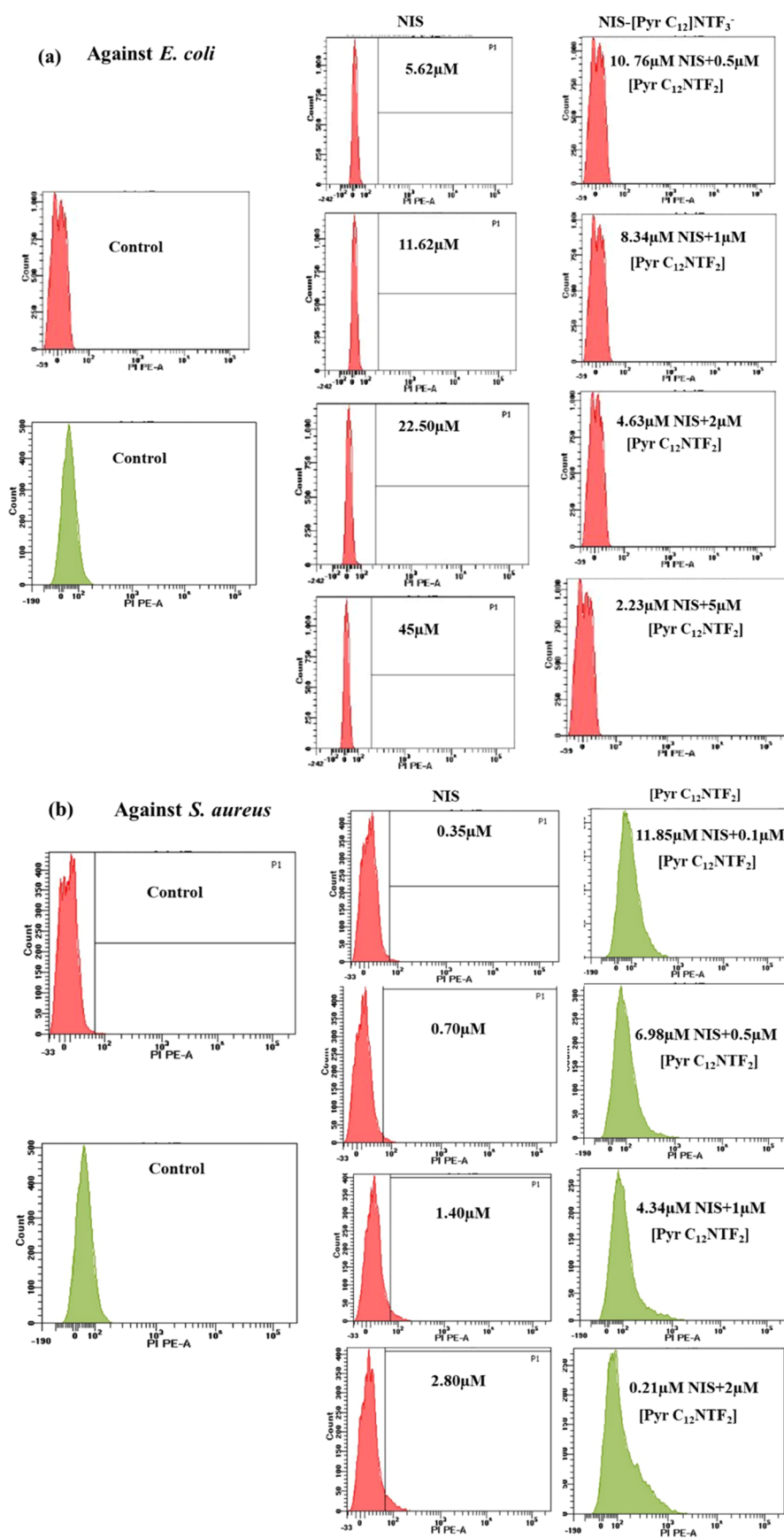
Figure 7. Flow cytometric analysis of (a) *E. coli* and (b) *S. aureus* treated with NIS and the conjugate, NIS−[Pyr C$_{12}$]NTF$_2$.
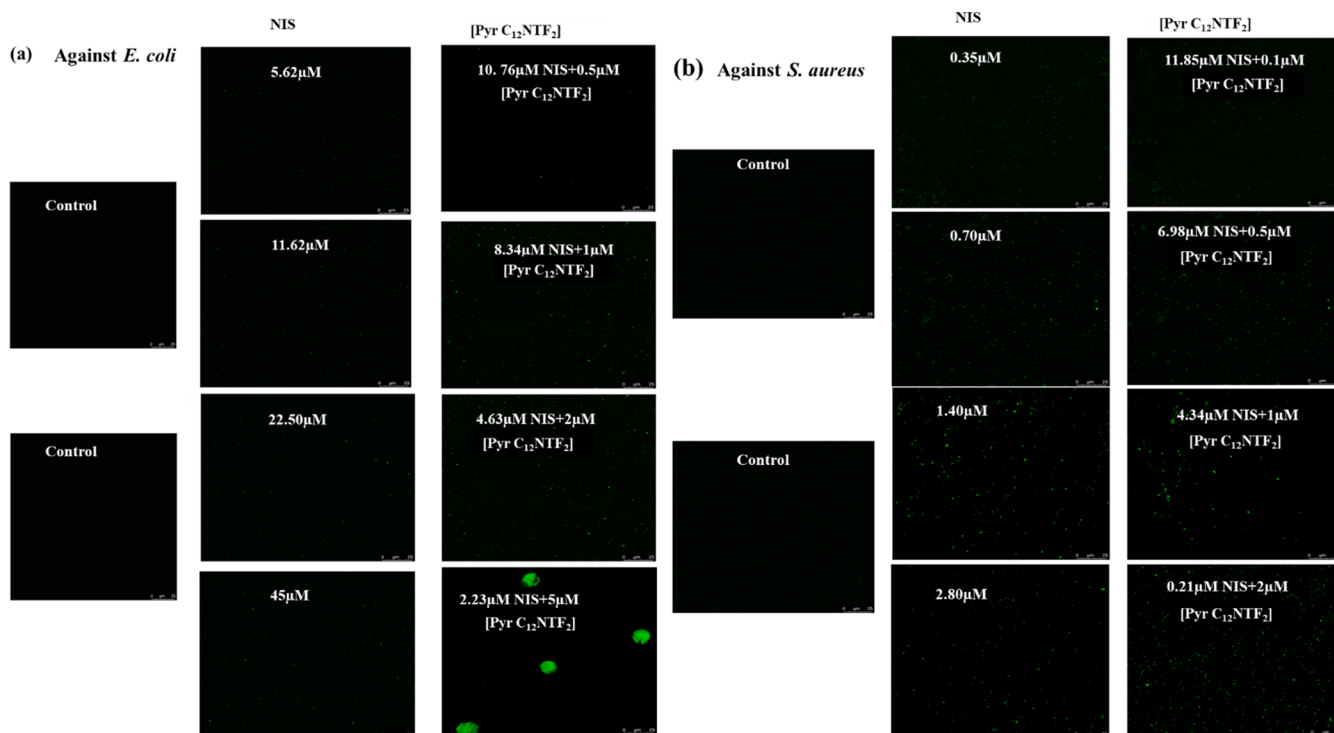
Figure 8. Confocal microscopy images of (a) *E. coli* and (b) *S. aureus* treated with NIS and a conjugate, NIS−[Pyr C$_{12}$]NTF$_2$.
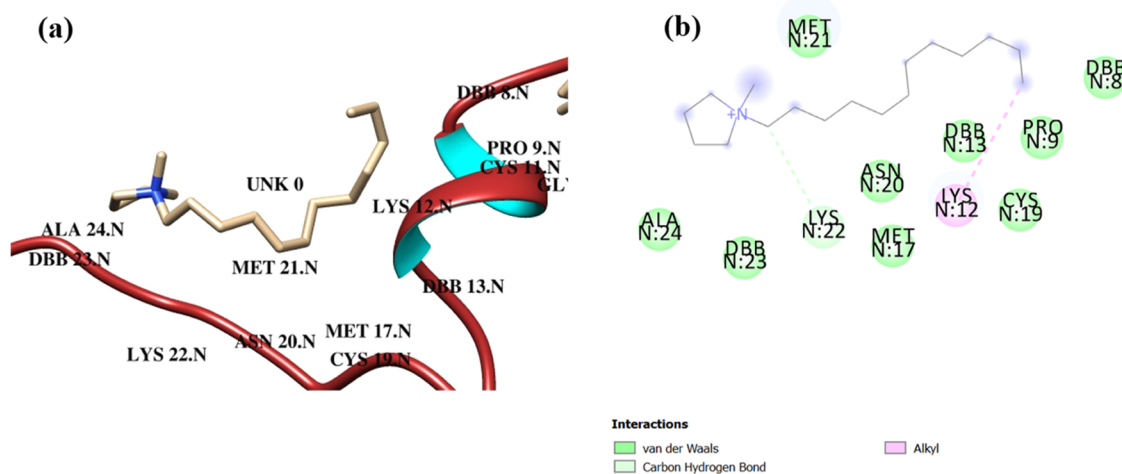
Figure 9. Schematic representation of NIS−[Pyr C$_{12}$]NTF$_2$ (highest binding energy) docked structures. (a) 3D representation of the NIS−[Pyr C$_{12}$]NTF$_2$ docked structure. (b) 2D notation of neighboring amino acids involved in the interaction.

3.3. Fluorescence-Activated Cell Sorting (FACS). Flow cytometry technique was employed to examine the rupturing of the cell membrane on treatment of strains with NIS and its conjugates. Propidium iodide (PI) is a well-known fluorescent agent that binds to DNA by intercalating into the bases with no specific base preference. PI is extensively used in analyzing the cell membrane.[16] Hence, the permeability of NIS and NIS−[Pyr C$_{12}$]NTF$_2$ was examined through the PI staining method. On the binding of PI with DNA, the quantum yield increases 20−30-fold, and its excitation is shifted to 535 nm (green) wavelength, which causes the generation of a signal upon staining.[27] The greater the inhibition, the greater the percentage of the PI signal. Figure 7a reveals that the damage to the cell membrane caused by NIS alone against *E. coli* was not significant, which suggests that the rupturing of the cell

membrane did not take place on increasing the concentration of NIS. Figure 7b shows the increasing PI signal depicting the damage to the cell membrane caused by NIS−[Pyr C$_{12}$]NTF$_2$ against *E. coli*. On comparing (Figure 7a,b), the rapid increase in the total percentage of PI-stained cells (positive cells)/dead cells in the case of conjugates suggests that the inhibition of bacterial cells took place through the rupture of the membrane, and the effect was more pronounced than that of NIS alone. This may be due to the increased hydrophobicity, which allows faster movement inside the cell through hydrophobic− hydrophobic interactions. However, the increase in PI-positive cells was much higher in the case of bacteria treated with NIS− [Pyr C$_{12}$]NTF$_2$ as compared to NIS, suggesting that the damage to the cell membrane was much higher when treated

with the NIS−[Pyr C_{12}]NTF$_2$ conjugate. This was further confirmed by confocal laser scanning microscopy (CLSM).

3.4. Confocal Laser Scanning Microscopy (CLSM). *E. coli* and *S. aureus* cells were treated with different concentrations of NIS and the NIS−[Pyr C_{12}]NTF$_2$ conjugate. The images of treated cells were captured under a microscope, as shown in Figure 8. The samples were analyzed under a fluorescence microscope. After the incubation of cells with PI, the control group showed the viability of the cells; the green color suggested the inhibition of cells in the presence of NIS and NIS−[Pyr C_{12}]NTF$_2$. Figure 8a shows that with an increasing concentration of NIS, the green color of cells was not as significant as it was in the FACs result. Similarly, Figure 8b shows that with an increasing concentration of ILs in NIS, the number of green-colored cells increased. On comparing the two, it was confirmed that in the presence of ILs, the membrane disruption was much higher as compared to that with NIS alone, and this corroborates the results obtained from FACs results.

3.5. Molecular Docking. The computational approach is a very useful technique to explore the interactions occurring between ligands and biomolecules (proteins/peptides).[21,28] It provides insights regarding the mode of interaction and also the binding sites of ligands on biomolecules, for instance, information regarding the binding between NIS and the ionic liquids used in this study. Out of 100 outcomes (conformers), depending upon the lowest binding energy, the best-fit conformation was selected and further analyzed using various visualizing software, viz., Chimera and Discovery Studio. The obtained binding energy for each system is presented in Table S1. The highest binding was found in the case of [Pyr C_{12}]NTF$_2$; hence, the best-fit conformation of NIS and [Pyr C_{12}]NTF$_2$ in Figure 9 shows the surrounding amino acids and mode of interaction involved in the complex formation. The molecular docking results show the involvement of PRO-9, LYS-12, MET-17, CYS-19, ASN-20, MET-21, LYS-22, and ALA-24. The obtained results suggest the involvement of van der Waals interactions and conventional hydrogen bonds in the complex formation. The binding energy obtained from molecular docking for the NIS−[Pyr C_{12}]NTF$_2$ system was found to be −10.58 kJ mol^{-1}. Further, a detailed analysis of the complex was performed using various techniques, which are discussed in the forthcoming sections.

3.6. Surface Tension. The surface tension technique was employed to determine the interaction occurring at the air/water interface. Figure S1 shows the surface tension plot of NIS in the presence of varied concentrations of [Pyr C_{12}]NTF$_2$ ranging from 0 to 0.72 mM in the absence and presence of NIS (50 μM). In Figure S1, the breaking point in both plots represents the CMC of ILs in the absence and presence of NIS (50 μM). The CMCs of [Pyr C_{12}]NTF$_2$ observed were 0.29 and 0.52 mM in the absence and presence of NIS, respectively. The CMC of [Pyr C_{12}]NTF$_2$ matched well with the reported literature.[12] In Figure S1, the surface tension of [Pyr C_{12}]NTF$_2$ in the presence of NIS increased as compared to that of [Pyr C_{12}]NTF$_2$ alone, which clearly indicates the binding of [Pyr C_{12}]NTF$_2$ with NIS due to the more hydrophobic environment at the air/water interface. In Table S2, the CMC value of [Pyr C_{12}]NTF$_2$ was found to increase in the presence of NIS; this is due to more adsorption of [Pyr C_{12}]NTF$_2$ on NIS and the development of more hydrophobic interactions between NIS−[Pyr C_{12}]NTF$_2$, revealing that the complex formed is less surface active.

Various other surface activity parameters were evaluated to further study the surface-active behavior of the complex formed between [Pyr C_{12}]NTF$_2$ and NIS. The surface pressure Π_{CMC} was calculated using eq 2.

$$\Pi_{CMC} = \gamma_0 - \gamma_{CMC} \tag{2}$$

where γ_0 and γ_{CMC} refer to the surface tension of water and ILs at the CMC, respectively. Π_{CMC} denotes the efficacy of the IL in reducing the surface tension of water. The calculated Π_{CMC} values are presented in Table S2. The increasing Π_{CMC} value of IL in the presence of NIS suggests that the complex formed between [Pyr C_{12}] NTF$_2$ and NIS has a lower tendency to decrease the surface tension and has less ability to adsorb on the air/water interface.

Further, Gibb's surface excess was calculated using eq 3.

$$\Gamma_{max} = -\frac{1}{2.303nRT}\left(\frac{d\gamma}{d\log C}\right) \tag{3}$$

where R refers to the universal gas constant whose value is taken as 8.314 J K^{-1} mol^{-1}, n is taken as 2 in the case of ILs because of the dissociation of IL into two ionic forms (cations and anions), and T refers to the experimental temperature, which was set to 298 K. The linear fit of the plot between surface tension and log concentration of IL yielded the value of $\left(\frac{d\gamma}{d\log C}\right)$. The values of Γ_{max} were calculated. Additionally, to evaluate the packing arrangement of the complex at the air/water surface, A_{min} was calculated using eq 4.

$$A_{min} = \frac{10^{20}}{N_A \Gamma_{max}} \tag{4}$$

where N_A is the Avogadro number and is taken as 6.023 × 10^{23}, Γ_{max} is Gibb's surface excess as calculated above, and A_{min} is the minimum area occupied by one molecule at the air/water interface. The calculated values of Γ_{max} and A_{min} are presented in Table S2. The value of Γ_{max} for IL decreased in the presence of NIS, in contrast to the value of A_{min}, which increased, suggesting that the size of the complex formed is large and that it is loosely packed at the air/water interface.[21]

3.7. Turbidity. The turbidity of the samples was measured using UV−vis spectroscopy, which is directly related to the density and size of the particles in the sample that are responsible for the scattering of light.[25] Figure S2 shows the turbidity of NIS in the absence and presence of [Pyr C_{12}]NTF$_2$. Various processes are responsible for the change in turbidity, viz., the size of the particle, refractive index, sample color, and nano- and micro-aggregation due to particle interactions, which are ascribed to complex formation.[25] In the present study, with increasing concentration of the IL in the NIS solution, the turbidity increased up to a micellar concentration of 0.22 μM, which mostly depicts the interaction occurring between NIS and [Pyr C_{12}]NTF$_2$. Thereafter, on further addition of the IL, the turbidity remained constant, which might be due to the fewer binding possibilities of ILs on NIS. This was further confirmed by DLS measurements.

3.8. Dynamic Light Scattering Measurement. The analysis of aggregate size in terms of the hydrodynamic diameter (D_h) of NIS and the NIS−[Pyr C_{12}]NTF$_2$ conjugate in phosphate buffer (10 mM, 7.4 pH) was performed using the DLS technique. Figure S3 shows the particle size of NIS in the absence and presence of [Pyr C_{12}]NTF$_2$. The particle size

analysis shows the interaction occurring between NIS and [Pyr C_{12}]NTF$_2$. Figure S3 shows the particle size of NIS in the absence and presence of [Pyr C_{12}]NTF$_2$. The diameter of NIS obtained was 143.31 nm. The overall increase in the size was observed to be 247.47 nm conclusively with increasing concentration of IL. The increasing particle size of NIS in the presence of IL suggests that NIS aggregates in the presence of IL due to the interaction prevailing between NIS and IL, which leads to the increasing size of the particle.

3.9. Circular Dichroism Spectroscopy. The secondary structure of NIS in the absence and presence of [Pyr C_{12}]NTF$_2$ was investigated in phosphate buffer (10 mM, 7.4 pH). Figure 10 shows the far-UV CD spectra of NIS. The CD
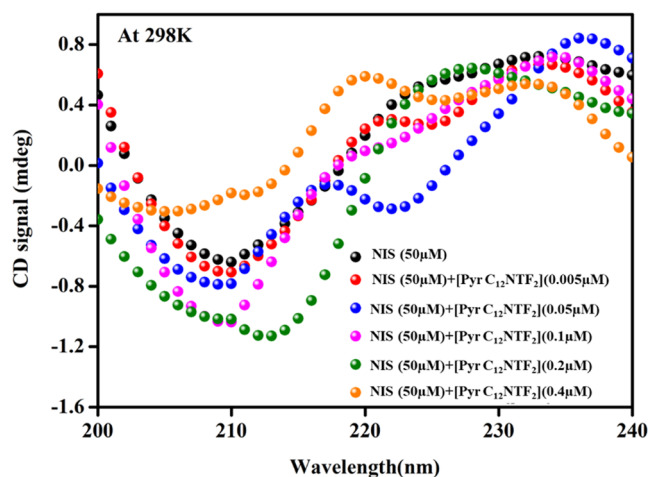
Figure 10. Far-UV CD spectra of NIS in the absence and presence of [Pyr C_{12}] NTF$_2$ at 298 K and 7.4 pH.

spectra show two negative peaks at 208 and 222 nm, which are clear evidence of the α-helix conformation of the peptide, as reported in the literature.[29] With increasing concentration of [Pyr C_{12}]NTF$_2$ in NIS, the negative CD signal increased at 208 nm, indicating the increasing α-helix conformation up to 0.2 μM concentration. However, beyond 0.2 μM concentration of [Pyr C_{12}]NTF$_2$, NIS loses its stability, and the α-helix conformation gets changed.[30]

3.10. Hemocompatibility. To investigate the compatibility of the designed conjugates, the hemocompatibility assay was performed using fluorescence, absorption, and far-UV CD spectroscopy. The fluorescence spectra of HSA in the absence and presence of NIS and its conjugate with [Pyr C_{12}]NTF$_2$ were recorded at 298 K. Trp is an intrinsic fluorophore present in HSA, which is responsible for fluorescence.[12] Figure S4(b) shows the maximum emission peak of HSA at 342 nm, which is a characteristic peak of Trp (fluorophor).[28] Any change in the fluorescence signal indicates the conformational change occurring in the protein due to interaction with ligands. The emission spectra of HSA in the presence of NIS and the NIS–IL conjugate do not show any shift in the maximum wavelength, which reveals that the polarity of the Trp remains unchanged,[12] while increasing fluorescence intensity reveals the complex formation between HSA and NIS (HSA and NIS–[Pyr C_{12}]NTF$_2$). The band in the absorption spectra at 280 nm indicates the presence of the α-helix structure in HSA, as shown in Figure S4(a).[21,24] The UV–vis spectra showed no shift in the UV–vis absorption band, which indicates that the secondary structure of HSA remains unchanged in the

presence of NIS and its conjugates with ILs. To further speculate any change in the secondary structure, far-UV CD spectra of the same set of samples were obtained. The far-UV CD spectra are shown in S4(c). The change in ellipticity was not significant but rather provided stability to the secondary structure of HSA.[12] The results from far-UV CD spectra were found to be consistent with the results obtained by fluorescence and UV–visible spectroscopy. Therefore, it can be concluded from the above results that the combinations of NIS and ILs are hemocompatible and can be used for developing therapeutic agents.

4. DISCUSSION

The escalating pervasiveness of multidrug resistance has led to an urgent need for alternative drugs and knowledge of their mechanism of action. Antibiotic combinations are currently the most effective therapy for treating various infections occurring due to microbes, such as malaria, tuberculosis, leprosy, etc.[31] Antimicrobial peptides (AMPs) have been explored as potential candidates for developing new antibiotics because they possess the least drug resistance and high antibacterial activity. Nisin Z is a well-known AMP, and it exhibits antibacterial, antiprotozoal, and antifungal activities.[32] Earlier studies showed the NIS is inactive against Gram-negative bacteria, such as *E. coli* strains, but active against Gram-positive bacteria.[30] ILs have emerged as antimicrobial agents against a wide range of microorganisms.[33,34] The toxicity of ILs has always been a serious concern for researchers while using them in developing therapeutic agents. Hence, in this study, we employed pyrrolidinium-based ILs because they are known to have less toxicity compared to other available ILs. The ILs were synthesized, and their toxicities were also determined, as reported in our previous publication.[12] The complex formation between the NIS and ILs was studied using the molecular docking method. The highest binding was observed in the case of ILs with the highest carbon chain length and NIS. This may be due to the van der Waals interactions occurring between the IL, [Pyr C_{12}] NTF$_2$, and NIS. Further, DLS, turbidity studies, and CD spectroscopy showed successful stable complex formation. Far-UV CD results suggested that ILs do not have any adverse effects on the conformation of NIS. For the antibacterial assay, a combination of ILs with an antimicrobial peptide (NIS) was tested against *E. coli* and *S. aureus*. The composition of ILs + NIS was highly effective in inhibiting the strains at lower concentrations than that of NIS alone, and it was effective even against a bacterial burden of *E. coli* that could not be inhibited by NIS, as shown in Figures 2–6. Interestingly, the increased efficacy of NIS in the presence of ILs tends to minimize the requirement for higher dosages of NIS, which is one of the major reasons for bacterial resistance as well as toxicity. The strongest antibacterial effect was seen in the case of ILs with a dodecyl carbon chain at the N atom of the pyrrole ring, which caused the maximum reduction of NIS concentration, consistent with the reported literature.[12,21,30,32,34] The increased efficacy of NIS in the presence of ILs containing a longer carbon chain length confirms the hypothesis that the addition of IL enhances (due to a higher surface activity of ILs, which are known for their adsorption tendency) the ability of NIS to enter the cell and maintain the level within the cell, leading to cell death.[35] FACS and confocal analysis showed the membrane-rupturing tendency of the complex tested on *E. coli* and *S. aureus*. Additionally, a hemocompatibility test of NIS and its complexes on human

serum albumin was performed, which confirmed the hemocompatibility of the complex with HSA. The increasing efficacy of NIS using ILs is not yet known, especially against *E. coli*; for the first time, we hereby report the remarkable results obtained in our study, which reveal that the combination of ILs and NIS might help in developing a new class of therapeutic agents.

5. CONCLUSIONS

In the present study, binding study results revealed stable complex formation between NIS and ILs. Further, NIS alone was found to be ineffective against *E. coli*, as previously reported, but a combination of NIS with pyrrolidinium-based ILs was found to be effective in inhibiting the growth of Gram-negative bacteria (*E. coli*) as well as *S. aureus*, which is a novel finding of our study. The inhibition of bacterial growth in the presence of the best combinations of 2.23 μM NIS + 5 μM [Pyr C$_{12}$] NTF$_2$ against *E. coli* and 0.21 μM NIS + 2 μM [Pyr C$_{12}$] NTF$_2$ against *S. aureus* was more than 95%. Further, flow cytometry and confocal techniques revealed that the best composition obtained killed the cells by rupturing the membrane integrity, leading to cell death. Taken together, the combination of NIS and ILs shows potential for further research. Moreover, the use of a combination of NIS and ILs could be a promising strategy to counter the increasing bacterial resistance.

■ ASSOCIATED CONTENT

ⓢ Supporting Information

The Supporting Information is available free of charge at https://pubs.acs.org/doi/10.1021/acsomega.3c07824.

Surface tension plot, DLS plot, UV−vis spectra, and far-UV CD spectra (PDF)

■ AUTHOR INFORMATION

Corresponding Author

Rajan Patel − *Biophysical Chemistry Laboratory, Centre for Interdisciplinary Research in Basic Sciences, Jamia Millia Islamia, New Delhi 110025, India;* ⓞ orcid.org/0000-0002-3811-2898; Phone: +91 8860634100; Email: rpatel@jmi.ac.in; Fax: +91 11 26983409

Authors

Juhi Saraswat − *Biophysical Chemistry Laboratory, Centre for Interdisciplinary Research in Basic Sciences, Jamia Millia Islamia, New Delhi 110025, India*

Ahmad Firoz − *Department of Biological Sciences, Faculty of Science, King Abdulaziz University, Jeddah 21589, Saudi Arabia; Princess Dr. Najla Bint Saud Al-Saud Centre for Excellence Research in Biotechnology, King Abdulaziz University, Jeddah 21589, Saudi Arabia*

Majid Rasool Kamli − *Department of Biological Sciences, Faculty of Science, King Abdulaziz University, Jeddah 21589, Saudi Arabia*

Complete contact information is available at:
https://pubs.acs.org/10.1021/acsomega.3c07824

Notes

The authors declare no competing financial interest.

■ ACKNOWLEDGMENTS

■ REFERENCES

(1) Tong, Z.; Zhang, Y.; Ling, J.; Ma, J.; Huang, L.; Zhang, L. An in vitro study on the effects of nisin on the antibacterial activities of 18 antibiotics against Enterococcus faecalis. *PLoS One* **2014**, *9* (2), No. e89209.

(2) Lewies, A.; Wentzel, J. F.; Jordaan, A.; Bezuidenhout, C.; Du Plessis, L. H. Interactions of the antimicrobial peptide nisin Z with conventional antibiotics and the use of nanostructured lipid carriers to enhance antimicrobial activity. *Int. J. Pharm.* **2017**, *526* (1−2), 244−253.

(3) Hadley, E. B.; Hancock, R. E. W. Strategies for the discovery and advancement of novel cationic antimicrobial peptides. *Curr. Top. Med. Chem.* **2010**, *10* (18), 1872−1881.

(4) Garcia, M. T.; Ribosa, I.; Perez, L.; Manresa, A.; Comelles, F. Micellization and antimicrobial properties of surface-active ionic liquids containing cleavable carbonate linkages. *Langmuir* **2017**, *33* (26), 6511−6520.

(5) Severina, E.; Severin, A.; Tomasz, A. Antibacterial efficacy of nisin against multidrug-resistant Gram-positive pathogens. *J. Antimicrob. Chemother.* **1998**, *41* (3), 341−347.

(6) Kiss, I.; Márialigeti, K.; Zukál, E.; Makk, J. Method for measurement of antibacterial activity of Nisin. *Bull. Univ. Agric. Sci. Vet. Med. Cluj-Napoca, Anim. Sci. Biotechnol.* **2007**, *63*, No. 64.

(7) Mulders, J. W. M.; Boerrigter, I. J.; Rollema, H. S.; Siezen, R. J.; de vos, W. M. Identification and characterization of the lantibiotic nisin Z, a natural nisin variant. *Eur. J. Biochem.* **1991**, *201* (3), 581−584.

(8) Bartoloni, A.; Mantella, A.; Goldstein, B.; Dei, R.; Benedetti, M.; Sbaragli, S.; Paradisi, F. In-vitro activity of nisin against clinical isolates of Clostridium difficile. *J. Chemother.* **2004**, *16* (2), 119−121.

(9) Dosler, S.; Gerceker, A. A. In vitro activities of nisin alone or in combination with vancomycin and ciprofloxacin against methicillin-resistant and methicillin-susceptible Staphylococcus aureus strains. *Chemotherapy* **2012**, *57* (6), 511−516.

(10) Zhang, Y.; Zhen, B.; Li, H.; Feng, Y. Basic ionic liquid as catalyst and surfactant: green synthesis of quinazolinone in aqueous media. *RSC Adv.* **2018**, *8* (64), 36769−36774.

(11) Frade, R. F.; Afonso, C. A. Impact of ionic liquids in environment and humans: an overview. *Hum. Exp. Toxicol.* **2010**, *29* (12), 1038−1054.

(12) Saraswat, J.; Wani, F. A.; Dar, K. I.; Rizvi, M. M. A.; Patel, R. Noncovalent conjugates of ionic liquid with antibacterial peptide melittin: an efficient combination against bacterial cells. *ACS Omega* **2020**, *5* (12), 6376−6388.

(13) (a) Jorgensen, J. H.; Hindler, J. F.; Reller, L. B.; Weinstein, M. P. New consensus guidelines from the Clinical and Laboratory Standards Institute for antimicrobial susceptibility testing of infrequently isolated or fastidious bacteria. *Clin. Infect. Dis.* **2007**, *44* (2), 280−286. (b) Wikler, M. A. Methods for dilution antimicrobial susceptibility tests for bacteria that grow aerobically: approved standard. *CLSI (NCCLS)* **2006**, *26*, No. M7-A7.

(14) Elshikh, M.; Ahmed, S.; Funston, S.; Dunlop, P.; McGaw, M.; Marchant, R.; Banat, I. M. Resazurin-based 96-well plate micro-dilution method for the determination of minimum inhibitory concentration of biosurfactants. *Biotechnol. Lett.* **2016**, *38* (6), 1015−1019.

(15) Akbari, R.; Hakemi-Vala, M.; Pashaie, F.; Bevalian, P.; Hashemi, A.; Bagheri, K. P. Highly synergistic effects of melittin with conventional antibiotics against multidrug-resistant isolates of acinetobacter baumannii and pseudomonas aeruginosa. *Microb. Drug Resist.* **2019**, *25* (2), 193−202.

(16) Lyu, Y.; Yang, Y.; Lyu, X.; Dong, N.; Shan, A. Antimicrobial activity, improved cell selectivity and mode of action of short PMAP-36-derived peptides against bacteria and Candida. *Sci. Rep.* **2016**, *6* (1), No. 27258.

(17) Seyedjavadi, S. S.; Khani, S.; Eslamifar, A.; Ajdary, S.; Goudarzi, M.; Halabian, R.; Akbari, R.; Zare-Zardini, H.; Fooladi, A. A. I.; Amani, J.; Razzaghi-Abyaneh, M. The antifungal peptide MCh-AMP1 derived from Matricaria chamomilla inhibits Candida albicans growth via inducing ROS generation and altering fungal cell membrane permeability. *Front. Microbiol.* **2020**, *10*, No. 3150.

(18) Saraswat, J.; Aldahmash, B.; AlOmar, S. Y.; Imtiyaz, K.; Rizvi, M. M. A.; Patel, R. Synergistic antimicrobial activity of N-methyl substituted pyrrolidinium—based ionic liquids and melittin against Gram-positive and Gram-negative bacteria. *Appl. Microbiol. Biotechnol.* **2020**, *104*, 110465−10479.

(19) Saraswat, J.; Singh, P.; Patel, R. A computational approach for the screening of potential antiviral compounds against SARS-CoV-2 protease: Ionic liquid vs herbal and natural compounds. *J. Mol. Liq.* **2021**, *326*, No. 115298.

(20) Kumari, M.; Maurya, J. K.; Tasleem, M.; Singh, P.; Patel, R. Probing HSA-ionic liquid interactions by spectroscopic and molecular docking methods. *J. Photochem. Photobiol., B* **2014**, *138*, 27−35.

(21) Mataraci, E.; Dosler, S. In vitro activities of antibiotics and antimicrobial cationic peptides alone and in combination against methicillin-resistant Staphylococcus aureus biofilms. *Antimicrob. Agents Chemother.* **2012**, *56* (12), 6366−6371.

(22) Tong, Z.; Zhang, Y.; Ling, J.; Ma, J.; Huang, L.; Zhang, L. An in vitro study on the effects of nisin on the antibacterial activities of 18 antibiotics against Enterococcus faecalis. *PLoS One* **2014**, *9* (2), No. e89209.

(23) Ahmed, S. A.; Rahman, A. A.; Elsayed, K. N.; El-Mageed, H. A.; Mohamed, H. S.; Ahmed, S. Dynamics. Cytotoxic activity, molecular docking, pharmacokinetic properties and quantum mechanics calculations of the brown macroalga Cystoseira trinodis compounds. *J. Biomol. Struct. Dyn.* **2020**, 3855−3873.

(24) Patel, R.; Saraswat, J. Effect of imidazolium-based ionic liquid on the antibacterial activity of an expired drug rifampicin. *J. Mol. Liq.* **2021**, *340*, No. 116844.

(25) Zhan, F.; Yang, J.; Li, J.; Wang, Y.; Li, B. Characteristics of the interaction mechanism between tannic acid and sodium caseinate using multispectroscopic and thermodynamics methods. *Food Hydrocolloids* **2018**, *75*, 81−87.

(26) Lau, M.; Tang, J.; Paulson, A. Texture profile and turbidity of gellan/gelatin mixed gels. *Food Res. Int.* **2000**, *33* (8), 665−671.

(27) Yang, D. D.; Paterna, N. J.; Senetra, A. S.; Casey, K. R.; Trieu, P. D.; Caputo, G. A.; Vaden, T. D.; Carone, B. R. Synergistic interactions of ionic liquids and antimicrobials improve drug efficacy. *iScience* **2021**, *24* (1), No. 101853.

(28) Maurya, N.; Maurya, J. K.; Singh, U. K.; Dohare, R.; Zafaryab, M.; Rizvi, M. M. A.; Kumari, M.; Patel, R. In vitro cytotoxicity and interaction of noscapine with human serum albumin: Effect on structure and esterase activity of HSA. *Mol. Pharmaceutics* **2019**, *16* (3), 952−966.

(29) Reinhardt, A.; Horn, M.; Schmauck, J. P. g.; Brohl, A.; Giernoth, R.; Oelkrug, C.; Schubert, A.; Neundorf, I. Novel imidazolium salt−peptide conjugates and their antimicrobial activity. *Bioconjugate Chem.* **2014**, *25* (12), 2166−2174.

(30) Sangcharoen, N.; Klaypradit, W.; Wilaipun, P.; Resources, N. Antimicrobial activity optimization of nisin, ascorbic acid and ethylenediamine tetraacetic acid disodium salt (EDTA) against Salmonella enteritidis ATCC 13076 using response surface methodology. *Agric. Nat. Resour.* **2017**, *51* (5), 355−364.

(31) Omidvar, Z.; Asoodeh, A.; Chamani, J. Studies on the antagonistic behavior between cyclophosphamide hydrochloride and aspirin with human serum albumin: time-resolved fluorescence spectroscopy and isothermal titration calorimetry. *J. Solution Chem.* **2013**, *42* (5), 1005−1017.

(32) Jančič, U.; Gorgieva, S. Bromelain and Nisin: The Natural Antimicrobials with High Potential in Biomedicine. *Pharmaceutics* **2022**, *14* (1), No. 76.

(33) Cornellas, A.; Perez, L.; Comelles, F.; Ribosa, I.; Manresa, A.; Garcia, M. T. Self-aggregation and antimicrobial activity of imidazolium and pyridinium based ionic liquids in aqueous solution. *iScience* **2011**, *355* (1), 164−171.

(34) Pendleton, J. N.; Gilmore, B. F. The antimicrobial potential of ionic liquids: A source of chemical diversity for infection and biofilm control. *Int. J. Antimicrob. Agents* **2015**, *46* (2), 131−139.

(35) Kohn, E. M.; Lee, J. Y.; Calabro, A.; Vaden, T. D.; Caputo, G. A. Heme dissociation from myoglobin in the presence of the zwitterionic detergent N, N-Dimethyl-N-Dodecylglycine betaine: Effects of ionic liquids. *Biomolecules* **2018**, *8* (4), No. 126.